Chaotic states and routes to chaos in the forced pendulum

D. D'Humieres, M. R. Beasley,* B. A. Huberman,† and A. Libchaber
Groupe de Physique des Solides, Ecole Normale Superieure, 24 rue Lhomond, 75231 Paris, Cedex 05, France
(Received 17 June 1982)

An experimental study of the chaotic states and the routes to chaos in the driven pendulum as simulated by a phase-locked-loop electronic circuit is presented. For a particular value of the quality factor ($Q=4$), for which the chaotic behavior is found to be rich in structure, the state diagram (phase locked or unlocked) is established as a function of driving frequency and amplitude, and the nature of the chaos in these states is investigated and discussed in light of recent models of chaos in dynamical systems. The driven pendulum is found to exhibit symmetry breaking as a precursor to the period-doubling route for chaos. Although period doubling is found to be fairly common in the phase-locked states of the pendulum, it does not always manifest itself in complete bifurcation cascades. Intermittent behavior between two unstable phase-locked states is also commonly observed.

I. INTRODUCTION

Recently a large number of theoretical calculations, simulations, and experiments have been carried out on various nonlinear systems in an effort to understand chaos and the routes to chaos in such systems. In this paper we present the results of an investigation of the forced pendulum, for which the control parameters are the driving amplitude and frequency. As is well known, the forced pendulum is isomorphic to many other familiar nonlinear systems, such as Josephson junctions and the phase-locked-loop configuration of a voltage-controlled oscillator, or VCO. In fact, the experimental work reported here was carried out using a phase-locked loop. Our study was stimulated by the earlier work of Huberman, Crutchfield, and Packard[1] and of Kautz[2] who have also studied this problem in the context of Josephson junctions.

It is essential to point out right at the outset that the seemingly simple situation of a forced pendulum is quite complex due to the fact that the space of variables is large. Besides the driving amplitude (which can have a dc component or bias in addition to the ac drive) and the driving frequency, one has the resonant frequency Ω_0 and the quality factor Q of the pendulum as important parameters. Indeed, it is the interplay between the driving force and the natural modes of the pendulum that results in chaos. Moreover, because of the periodic nature of the restoring potential, both running and oscillatory motions are possible. In order to deal as simply as possible with such complexity in this paper, we first establish the "state" diagram of the forced pendulum as a function of the driving amplitude and frequency for a particular value of Q where the chaotic behavior is found to have rich structure. We then establish the nature of these states (e.g., phase locked or not, periodic or chaotic) and investigate the nature of transitions between them.

In broad outline our results are in agreement with the earlier work of Huberman *et al.*,[1] and Kautz,[2] but much more complete in the zero-bias case. In particular, we have found some new results of interest. They are as follows:

(a) Prior to going chaotic the pendulum is found to break its spatial symmetry and oscillate with a larger amplitude to one side than the other. This symmetry-breaking phenomenon appears to be an inherent part of the period-doubling cascade in this particular system.

(b) The period-doubling cascade is found to be a generic phenomena for the forced pendulum. It occurs in the oscillating states of the pendulum but also in the rotating regime where the pendulum rotation frequency is phase-locked to the driving frequency. In these cases the chaotic behavior is characterized by a power spectrum $S(\omega)$ peaked at each subharmonic of the drive frequency but $S(\omega)\rightarrow 0$ as $\omega\rightarrow 0$, implying that phase locking is maintained at dc.

(c) Another chaotic state commonly observed appears to be related to random transitions between two phase-locked states that have become unstable. The two states may be oscillating or rotating. In this case the chaotic behavior is characterized by a mean white-noise spectrum and hence is associated with the loss of phase locking.

(d) A third kind of chaotic behavior arises when the driving frequency is much smaller than the low-amplitude resonance frequency of the pendulum ($\Omega \ll \Omega_0$). If the amplitude of the driving force becomes larger than the critical value at which the pendulum begins to rotate, the motion is a combination of positive and negative rotations in between which the pendulum undergoes damped oscillations. The ensuing sensitivity on initial conditions for every rotation leads to a chaotic state with a white-noise spectrum.

The main body of this paper is organized as follows. In Sec. II we review the equations of motion of the forced pendulum, establishing notation and providing a correspondence between several useful isomorphisms. Next, we establish the state diagram (Sec. III) followed by a discussion of the various transitions between these states and the routes to chaos we observed (Secs. IV and V). The details of the actual experimental equipment and procedures are contained in the appendixes, along with some of the mathematical details of the theoretical interpretations.

II. EQUATIONS OF MOTION FOR THE FORCED PENDULUM

The equation of motion for the forced pendulum is of the form

$$a\ddot{\theta}+b\dot{\theta}+c\sin\theta=\Gamma(t)\ , \tag{1}$$

where a is the moment of inertia, b the damping constant, $c\sin\theta$ the restoring torque, and $\Gamma(t)$ the driving torque. The corresponding variables for pendula, Josephson junctions, and phase-locked loops are given in Table I for convenience, as it is frequently helpful from the physical point of view to use the "language" of these various systems in discussing our results. Specifically, for a phase-locked loop, such as the one used in our experimental work, the accessible variables are the summing voltage V and the feedback current $I_{\rm FB}$, which are proportional to $\dot{\theta}$ and $\sin\theta$, respectively.

As usual, it is convenient to transform this equation into dimensionless form. The two characteristic times are $\tau_0=b/c$ and $\Omega_0^{-1}=(c/a)^{-1/2}$, where τ_0 is the exponential damping time for the highly viscous pendulum (i.e., when the $\ddot{\theta}$ term can be neglected) and Ω_0 is the low-amplitude natural oscillatory frequency of the undamped pendulum. This leads to two possible dimensionless equations:

$$\beta\ddot{\theta}+\dot{\theta}+\sin\theta=\gamma(\tau) \tag{2}$$

or

$$\ddot{\theta}+\frac{1}{Q}\dot{\theta}+\sin\theta=\gamma(\tau)\ , \tag{3}$$

where $\beta=Q^2=ac/b^2$, $\gamma(\tau)=\Gamma(\tau)/c$, and the time τ has been normalized by τ_0 and Ω_0^{-1} in Eqs. (1) and (2), respectively. In general, the forcing term (torque) is given by

$$\gamma(t)=\gamma_0+\gamma_1\cos\omega\tau+\gamma_N(\tau)\ , \tag{4}$$

where ω is the normalized frequency, γ_0 the dc forcing term, γ_1 the amplitude of the ac driving force, and γ_N is a noise term. In this work Q is fin-

TABLE I. Corresponding variables for pendula, Josephson junctions, and phase-locked loops.

	Pendulum	Josephson junction	Phase-locked loop
θ	Angular position	Quantum phase difference	Phase difference between the oscillators
$\dot{\theta}$	Angular velocity	$\frac{2\ eV}{\hbar}$	kV
a	Inertia momentum	$\hbar C/2e$	C/k
b	Viscous damping	$\hbar/2eR$	$1/kR$
$c\sin\theta$	Restoring torque	Josephson current I_J	Feedback current $I_{\rm FB}$
c		Critical current I_c	V_1/R_S
$\Gamma(t)$	Applied torque	Applied current $I(t)$	Applied current $V_E(t)/R_E$
$\Omega_0=\sqrt{c/a}$	Natural frequency	$(2eI_c/\hbar C)^{1/2}$	$(kV_1/R_SC)^{1/2}$
$\tau_0=b/c$	Damping time	$\hbar/2eRI_c$	R_S/kRV_1
$Q=(ac/b^2)^{1/2}$	Quality factor	$(2eI_cR^2C/\hbar)^{1/2}$	$(kV_1CR^2/R_S)^{1/2}$

ite and we shall use Eq. (3). However, in the limit of large damping $\beta=Q^2\rightarrow 0$, Eq. (2) is more appropriate.

III. STATE DIAGRAM OF THE FORCED PENDULUM

In order to provide a simple framework in which to understand our results, we present here the state diagram of the forced pendulum for the particular conditions we studied most carefully. The diagram was obtained directly from experiment by taking traces of the summing point voltage of our phase-locked loop (see Appendix A) as a function of the drive frequency for various amplitudes. A typical sequence of traces is shown in Fig. 1.

As can be readily seen, the pendulum exhibits two basic types of states: phase-locked states in which there are no fluctuations in $\dot{\theta}\propto V$ in the dc limit and unlocked states for which fluctuations are evident near dc. For example, consider the trace for $\gamma_1=1.5$, i.e., 1.5 times the critical torque. As the driving frequency is reduced, the system, initially in an oscillatory state phase locked to the driving frequency, breaks its symmetry and jumps to a new state in which it is still phase locked but now with a nonzero $\langle\dot{\theta}\rangle$. (As we shall see later, the symmetry is actually broken before the state change takes place.) The motion in this new state corresponds to a periodic running solution in which the pendulum rotates 2π successively each period of the driving force. The other phase-locked states are similar, involving only different numbers of net rotations in each driving period. These states are analogs of the zero-bias ac Josephson steps seen in Josephson junctions and follow the relation $\dot{\theta}\propto V=k^{-1}n\omega$ indicated by the straight lines in the figure, where n is an integer and k is the voltage-to-frequency conversion factor of the VCO. They are stable in the presence of small dc bias. Some higher-order steps are also seen at lower frequencies, as are occasional steps of the form $\dot{\theta}\propto V=k^{-1}(p/q)\omega$, where p and q are integers. The hysteresis present between decreasing and increasing frequency is shown by the arrows.

The unlocked states are clearly chaotic as shown by the finite noise power spectral density at dc evident in the figure. We should point out that they are not unrelated to the phase-locked ($V=k^{-1}n\omega$) states, however. For $\omega\lesssim 1$ they serve as the transitions between phase-locked states of different n, and at low frequencies the steps themselves ($n=0$ and 1 for $\gamma_1=1.5$) appear chaotic. The undulatory behavior seen at low frequencies in Fig. 1 persists to very low drive frequencies as is illustrated in Fig. 2, which shows the behavior in this region on an expanded scale. The overall state diagram that emerges from a complete family of traces such as these is shown in Fig. 3 for the particular case $Q=4$.

It is important to note that, whereas this state diagram is closely related to the bifurcation diagram

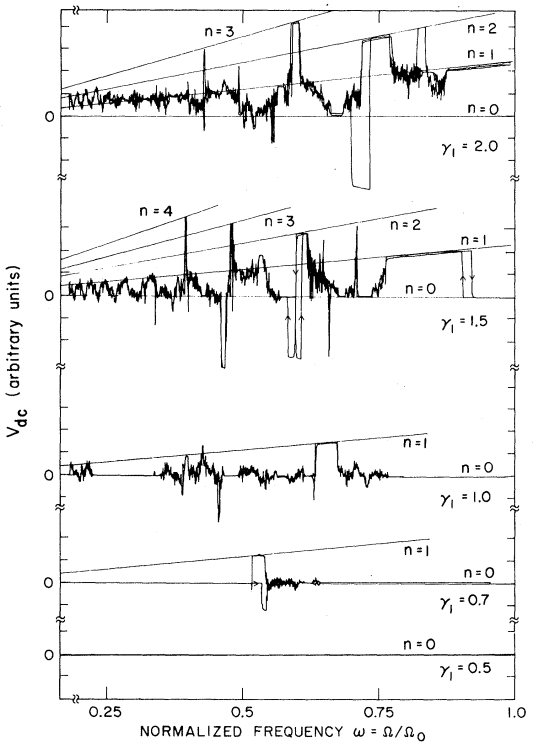

FIG. 1. Voltage fluctuations of the simulator circuit near dc as a function of the driving frequency for various driving amplitudes. Note pattern of phase-locked and -unlocked states. Straight lines indicate phase-locked steps satisfying the relationship $V=nk^{-1}\omega$.

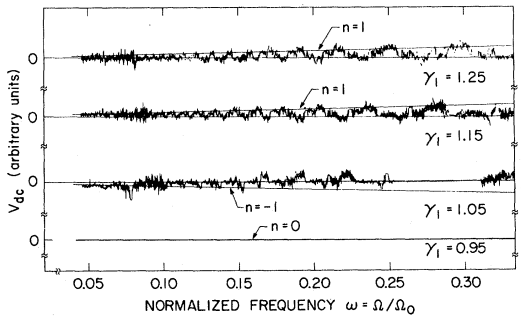

FIG. 2. Extension of the data of Fig. 1 to lower frequencies.

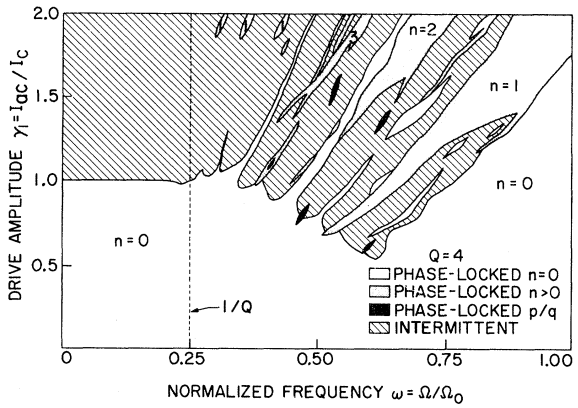

FIG. 3. State diagram for the driven pendulum with $Q=4$ and $\gamma_0=0$.

of Huberman *et al.*,[1] it is not exactly the same. Period-doubling cascades (pitchfork bifurcations) and their associated chaos are not seen in Figs. 1–3 because they have a noise power spectral density such that $S(\omega)\to 0$ as $\omega\to 0$. They do exist, however, and arise in the phase-locked states shown in Fig. 3. We shall return to this point later. The structure seen in Fig. 3 does clarify the content of the generally chaotic region noted by Huberman *et al.*,[1] although, as seen here, that region extends to much lower frequencies than found by those authors. Recent numerical simulations by Pedersen and Davidson[3] yield a similar qualitative picture.

IV. PHASE-LOCKED STATES

As seen in Fig. 3, phase-locked states occur at low ac drive and high frequencies ($n=0$) and in the form of stripes ($n\geq 0; n=p/q$) throughout the generally chaotic region at high drives and low frequencies. In this section we discuss the nature of the chaos observed in these phase-locked regions and of the transitions observed between the phase-locked states and the intermittent regions in Fig. 3.

A. Phase-locked oscillating states ($n=0$)

Consider first the large portions of $n=0$ region at low γ_1 and large ω where the motion is entirely contained in the first potential minimum. As discussed by Huberman *et al.*,[1] the basic response of a pendulum in this regime is that of a highly nonlinear oscillator for which, in the presence of sufficiently strong ac drive, the system exhibits chaos preceded by the period-doubling cascade analogous to that present in a single-well anharmonic oscillator.[4] This behavior is best understood by considering the response of a pendulum as a function of frequency of various ac drive amplitudes. The filtered (fundamental) amplitude response of our simulator as a function of ω for various γ_1 is shown in Fig. 4. The evolution of the phase-space portraits θ vs $\sin\theta$ (i.e., the signals I_{FB} and V from the phase-locked loop) for increasing γ_1 at fixed $\omega=0.67$ are illustrated in Figs. 5 and 6 along with the noise power spectra for those cases ($\gamma_1=0.54$ and 0.68) where the response is chaotic.

In order to interpret these results it is helpful to compare them with those expected from classical perturbation theory. In a linear analysis the solution to Eq. (3) can be written in the form

$$\theta=-\alpha\sin(\omega t-\phi)\,, \tag{5}$$

where

$$\alpha e^{-i\phi}=\frac{\gamma_1}{i(1-\omega^2)-\omega/Q} \tag{6}$$

leading to a resonance for $Q>1/\sqrt{2}$ at a frequency $\omega=(1-1/2Q^2)^{1/2}$ with a maximum amplitude

$$\alpha=\frac{\gamma_1 Q}{(1-1/4Q^2)^{1/2}}\,. \tag{7}$$

When the nonlinearity is included the problem becomes less trivial, but for small γ_1 it can still be described by a perturbation expansion. We consider solutions of the type

$$\theta=-\sum_{n=0}^{\infty}\alpha_{2n+1}\sin[(2n+1)\omega\tau-\phi_n] \tag{8}$$

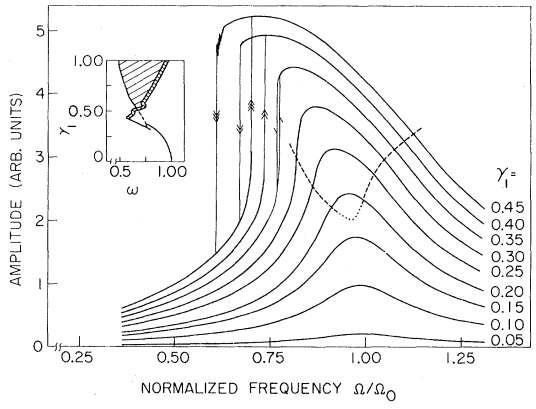

FIG. 4. Observed filtered (fundamental) amplitude response of the simulator circuit for various driving amplitudes. Dashed line shows domain of broken symmetry in the pendulum motion. Insert shows the observed bifurcation diagram similar to that reported in Ref. 1.

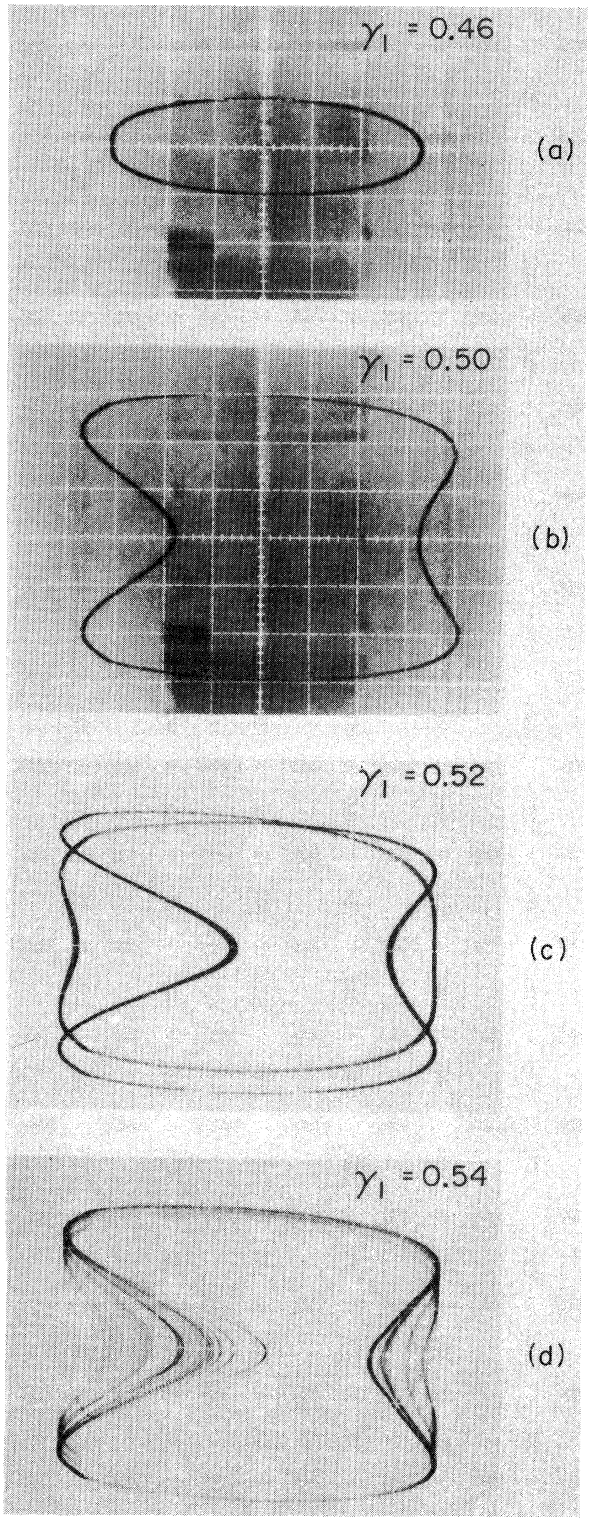

FIG. 5. (a) Evolution of the phase-space portraits ($\dot{\theta}$ vs $\sin\theta$) for increasing driving amplitude γ_1 at fixed frequency $\omega=0.67$. (b) Note the symmetry breaking, (c) followed by period doubling, (d) followed by chaos.

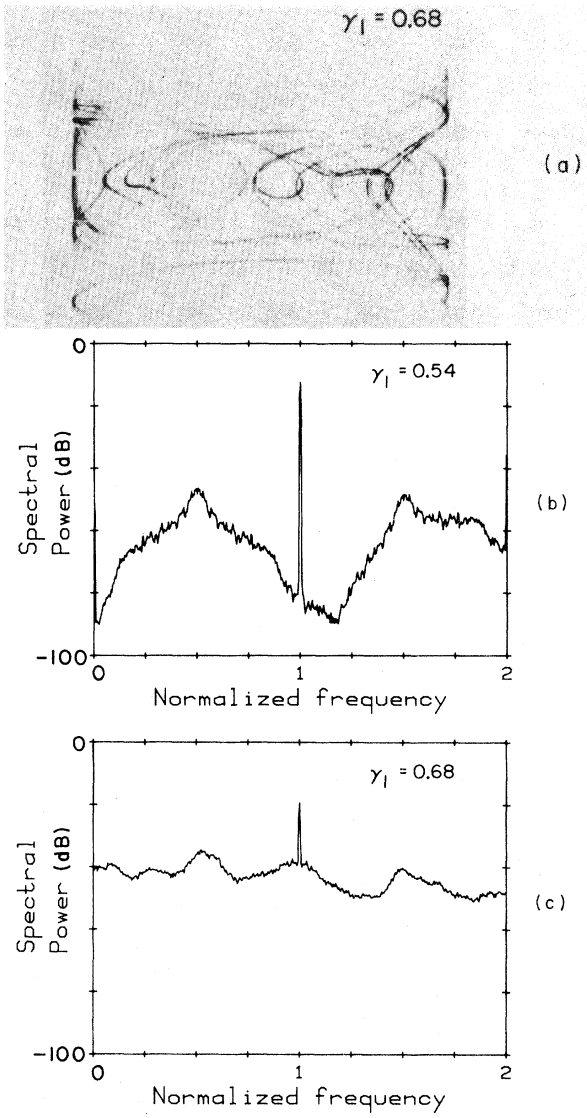

FIG. 6. (a) Phase-space portrait corresponding to the intermittent domain of Fig. 3 at $\omega=0.67$. (b) and (c) show the spectral power density corresponding to Figs. 4(d) and 5(a). Note different behavior as $\omega\rightarrow 0$. Note also that in this figure and all other power spectra the frequency axis is normalized to the drive frequency.

as it is easy to show that for small amplitudes the even terms do not appear. Limiting ourselves to the first-order terms we obtain

$$-\omega^2\alpha+2J_1(\alpha)=\gamma_1\sin\phi\ , \tag{9}$$

$$-\frac{\alpha\omega}{Q}=\gamma_1\cos\phi\ , \tag{10}$$

where the J_n are Bessel functions of the first kind. In Fig. 7 we show the numerical solution of Eqs. (9)

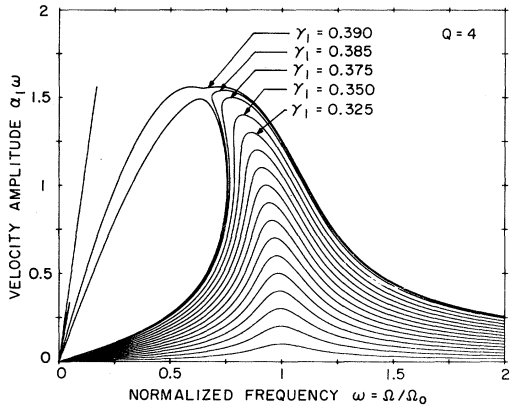

FIG. 7. Calculated fundamental response using perturbation theory as described in text.

and (10) for the amplitude of the velocity term $\dot{\theta}$ [i.e., $\alpha_1\omega$ as $\dot{\theta} = -\alpha_1\omega\cos(\omega\tau - \phi_1)$] as a function of ω for various drive amplitudes.

Comparing Figs. 4 and 7 we see that for $\gamma_1 < 0.385$ there is good agreement between the observed behavior and the results obtained with perturbation theory. We observe the usual nonlinear resonance shape, with a shift of the resonance peak to lower frequencies. Above a critical value $\gamma_1 \simeq 0.3$ the resonance becomes S shaped with three solutions, only two of which are stable, and hysteresis develops in the experimental curve.

Clearly, however, for $\gamma_1 \geq 0.39$ the simple analytical solution is no longer valid, since even including higher-order odd terms, it is not possible to explain the following two important phenomena which appear in the experiment:

(1) For $\omega \lesssim 1$ at the higher driving amplitudes the resonance curve shows a small distortion which is related to the generation of second harmonics. In fact, that is just the signature of a bifurcation of the pendulum at which an asymmetry appears in the angular motion. This asymmetry is clearly evident in the phase-space portrait of Fig. 5(b) and exists above the dashed line shown in Fig. 4. This symmetry breaking of the pendulum oscillations appears to be an unavoidable precursor of the period-doubling cascade for this system. This phenomena has been overlooked or ignored in previous discussions of chaos in symmetric anharmonic potentials. It is possible to analytically derive the onset of the symmetry breaking as shown in Appendix B.

(2) The period-doubling cascade also leaves its signature. In Fig. 4 it corresponds to the small region before the instability point of the S-shaped curve. The period-doubling cascade itself is shown both in the phase portraits of Fig. 5 and in the power spectrum of Fig. 6(b). For the sequence shown in these figures (increasing γ_1 at fixed $\omega = 0.67$), the transition at the end of the chaotic region associated with the period-doubling cascade is into an intermittent state [e.g., Figs. 6(a) and 6(c)]. The nature of this intermittent state will be discussed in greater detail in Sec. V.

We should note that in Figs. 5 and 6 the period-doubling cascade is incomplete, presumably due to noise in the phase-locked loop. Specifically, the asymptotic evolution of the cascade is not observed and the system goes directly into the chaotic region where the inverse cascade takes place. The signature of this inverse cascade can be seen in the power spectrum shown in Fig. 6(b), i.e., a noise spectrum peaked at each subharmonic of the drive frequency which goes to zero as $\omega \to 0$, as expected.

In general, we found that for low γ_1 and $0.6 \lesssim \omega \lesssim 1$, where the motion of the pendulum is entirely in one well, the $n=0$ state became unstable via the period-doubling route as found by Huberman *et al.*[1] (see inset of Fig. 4). The results of Fig. 5 are typical, although it was found that the application of a small dc bias often allowed us to go further into the cascade (e.g., to $\omega/8$). The reason for the greater stability in the presence of a bias is not completely understood but appears to reflect (at least in part) the effect of external symmetry breaking in preventing noise-driven transitions between the two equivalent symmetry-broken states at zero bias. At lower frequencies the transition from the $n=0$ state was discontinuous and not preceded by period doubling.

Within the generally chaotic regime of the state diagram, the striped regions with $n=0$ correspond to phase-locked oscillations with amplitudes sufficient to go beyond the first well, but in a symmetric fashion so as to result in $\langle\dot{\theta}\rangle = 0$. Two phase-space portraits and power spectra ($\omega = 0.67$; $\gamma_1 = 0.76$ and $\gamma_1 = 1.94$) typical of these regions are presented Fig. 8. The particular cases correspond to situations in which the pendulum rotates one time 2π and one time -2π, respectively, during three [8(a) and 8(b)] and one period [8(c) and 8(d)] of the ac drive, as shown by the corresponding noise spectra. Note that, as in Rayleigh-Bernard experiment,[5] or for the parametric pendulum,[6] the period tripling showed Figs. 8(a) and 8(b) occurs not in the chaotic region following the period-doubling cascade, but as an independent route to chaos. However, the transitions away from this period three state were observed to follow a period-doubling pattern (i.e., 3×2^n).

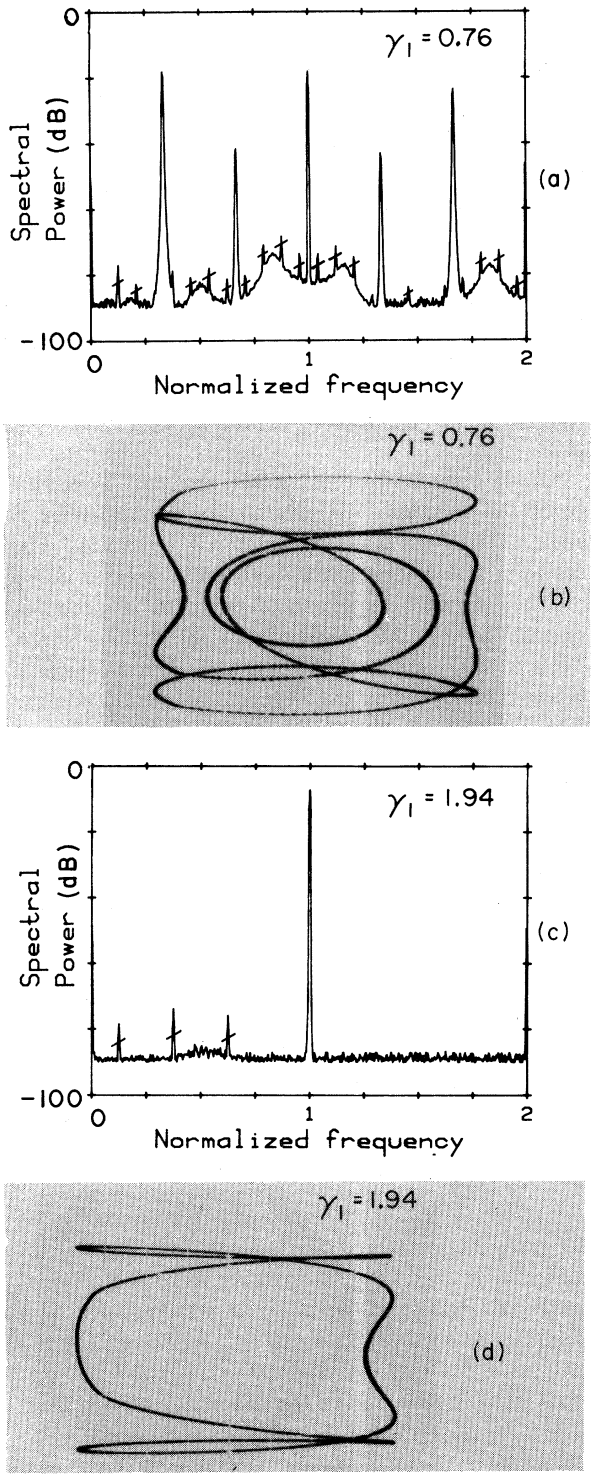

FIG. 8. Phase-space portraits and associated spectral power for two symmetric ($n=0$) large-amplitude rotating states. (a) and (b) correspond to a period-tripled state. (c) and (d) correspond to a simple period-one state. Note that the spectral lines with slash marks are due to 50-Hz pick-up.

B. Phase-locked rotating states ($n \geq 1$)

There are many phase-locked rotating (i.e., periodic running) states evident in Fig. 3. In general, we find that the behavior of the pendulum as one crosses such states (either in driving frequency or amplitude) is not universal in that no single pattern is observed. Period doubling is common place but not necessarily in the form of fully developed cascades. Consider, for example, the phase-space orbits shown in Fig. 9, which illustrate the evolution of the system as γ_1 is increased across the $n=2$ state at $\omega=0.67$. The basic structure of these orbits is very typical, other states differing essentially only in the number of loops on the top (or bottom) of the orbit. Each loop corresponds to a 2π rotation of the pendulum. Note, however, that as γ_1 increases monotonically, the orbits exhibit the sequence $\omega/2 \rightarrow \omega \rightarrow \omega/2$. This type of behavior is not understood but may simply reflect a nonmonotonic relationship between the physical control parameter γ_1 and that governing the pitchfork bifurcations in the Feigenbaum[7] theory based on the logistic equation.

In any event, it is clear from the phase-space orbits that the dynamics associated with period doubling is essentially the same for the $n=0$ and $n\neq 0$ states (compare Figs. 5 and 9.) The orbits differ only in the existence of loops on the orbit for $n > 1$. In particular, without exception period doubling is seen to arise when the velocity of the pendulum ($V \propto \dot{\theta}$) goes through zero just as the pendulum approaches the "up" position ($I \propto \sin\theta \rightarrow 0$).

In order to put the above ideas on a more mathematical basis, consider a perturbation-expansion solution of Eq. (3) for a phase-locked rotating state. Because of the phase locking, the solutions have the form

$$\dot{\theta} = n\omega - \omega \sum_{p=1}^{\infty} p\alpha_p \cos(p\omega\tau - \phi_p) \quad (\langle \dot{\theta} \rangle = n\omega) \tag{11}$$

and thus

$$\theta = \theta_0 + n\omega\tau - \sum_{p=1}^{\infty} \alpha_p \sin(p\omega\tau - \phi_p) \, . \tag{12}$$

To first order, the solution has been found by Pedersen *et al.*[8]:

$$\theta = \theta_0 + n\omega\tau - \alpha \sin(\omega\tau - \phi) \, . \tag{13}$$

Writing $\theta_n = \theta_0 + n\phi$ one obtains

$$\gamma_0 = J_n(\alpha)\sin\theta_n + n\omega/Q \, , \tag{14}$$

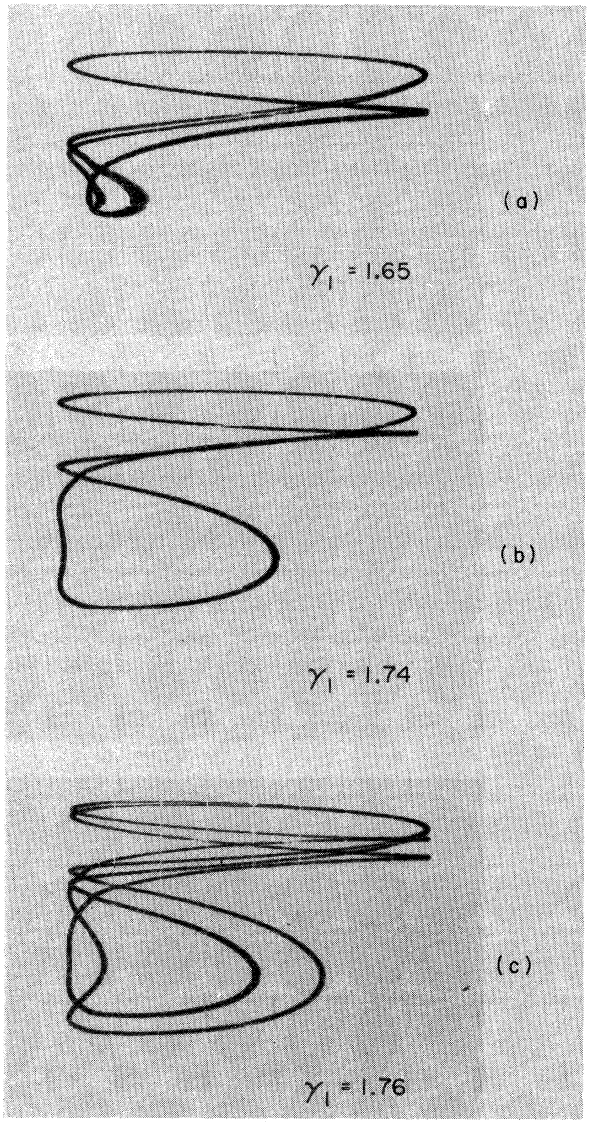

FIG. 9. Phase-space portraits of phase-locked periodic running states ($n \geq 1$) illustrating nonmonotonic period-doubling pitch fork bifurcations.

$$\gamma_1 e^{i\phi} = -\alpha \left[\frac{\omega}{Q} \left[1 + \frac{2n^2}{\alpha^2} \right] - \frac{2n}{\alpha^2}\gamma_0 + i \left[\omega^2 + \frac{2J_n'(\alpha)}{\alpha}\cos\theta_n \right] \right] . \quad (15)$$

Thus, we arrive at a set of three implicit equations [(14) and (15)] that cannot be solved analytically to obtain the unknowns α, ϕ, and θ_n. However, considering Eq. (13), we see that it implies that under the oscillating constraint the pendulum rotates with an angular frequency which is n times the driving frequency but with an angular velocity which is sinusoidally modulated by the term $\alpha \sin(\omega\tau + \phi)$. It is this term that is associated with the complex behavior of the pendulum, i.e., the period-doubling cascade.

One can develop this picture further and relate it to the period-doubling cascade of the phase-locked oscillating pendulum for $n=0$ and $\gamma_0=0$ [$\theta_0=0$ and Eq. (15) reduce to Eqs. (9) and (10)] described previously. Indeed, in Eq. (15) there are resonance terms for the imaginary and real parts of $\gamma_1 e^{i\phi}$. These nonlinear resonance terms presumably lead to the period-doubling cascade for reasons similar to the nonlinear resonance effects of the oscillating pendulum.

Going one step further we can analyze the stability of the solution (13). As shown in Appendix B such an analysis leads to Mathieu's equation. The essential point here is that both parameters a and q of the Mathieu equation depend in a complex manner on γ_1, the amplitude of the driving force. This is why one usually observes period-doubling phenomena which evolves in a nonmonotonic manner such as illustrated in Fig. 9. The forced pendulum is in this respect strikingly different from the parametric pendulum,[6] where the period-doubling cascade evolves fully. In this case, in the Mathieu equation for the stability of the solution, only the q term depends on the forcing amplitude and varies linearly with it. Thus, except for the $n=0$ state, the forced pendulum is not, in general, a simple system for displaying the period-doubling cascade.

V. NONPHASE-LOCKED STATES

A. Low-frequency regime

As seen in Fig. 3, the generally chaotic region of the state diagram extends down to low frequencies such that $\omega \ll 1$. This is in contrast to the original result of Huberman *et al.*,[1] in which there was found to be a cutoff at $\omega \simeq Q^{-1}$. Although the exact reason for this discrepancy is not known, it appears likely to be due to the simulator circuit used in Ref. 1, which was restricted in the number of 2π rotations it could simulate. We should point out, however, that some role of noise in inducing a chaotic response in this region can not be completely ruled out. In a similar vein, it is possible that transients due to the frequency sweep also play a role in the behavior observed. Finally, it should be noted that we did not determine exactly how low in

frequency this region extends.

On the basis of the traces in Fig. 2, we surmise that any structure in the state diagram in this region must be on a very fine scale and associated with the undulations between the $n=0$ and 1 states evident in the figure. This extreme sensitivity to the control parameters is also shown in Fig. 10, which shows the real-time response of our circuit and the associated noise spectra for two nearly identical values of γ_1. Note the striking 30-dB noise rise in going from 10(c) to 10(d) in a power spectrum that is otherwise the same. Note also the slight differences in the ringing down transients from cycle to cycle in Fig. 10(b) but not in Fig. 10(a).

Better insight into the nature of this behavior can be obtained by considering first the response of the pendulum to an applied dc bias. Since we are considering low ac drive frequencies, the motion of interest should be closely related to that at dc. This problem has been analyzed by McCumber[9] in the context of the resistively shunted junction (RSJ) model of Josephson junctions. The dc I-V (i.e., $\langle\dot{\theta}\rangle-\gamma_0$) curves obtained on our simulator corresponding to the situation studied by McCumber are shown in Fig. 11. The main features are as follows.

The asymptotic behavior for large γ_0 is such that $\langle\dot{\theta}\rangle=\gamma_0 Q$. In effect, for $\gamma_0 \gg 1$ the pendulum rotates at a high angular velocity, thus the nonlinear $\sin\theta$ term can be neglected in Eq. (1), and it is easy to show that the pendulum reaches a limiting angular velocity $\dot{\theta}=\gamma_0 Q$ in a time of order $1/Q$. For $Q \gtrsim 1$ the $\langle\dot{\theta}\rangle$ vs γ_0 curve exhibits hysteresis, which can be simply understood. When the torque is increased from zero to the critical value $\gamma_0=1$ because of the inertia term, the pendulum starts abruptly to rotate at an angular average velocity $\langle\dot{\theta}\rangle \simeq Q$. Upon decreasing the torque, the inertia of the pendulum causes it to keep rotating even for $\gamma_0<1$ down to a critical value γ_{0C}. At this critical value of γ_0 the pendulum reaches the unstable position with zero velocity; from there it relaxes toward a stable equilibrium position through a damped limit cycle with a characteristic time $\tau=Q/\Omega_0$. The critical torque value γ_{0C} has been calculated numerically by McCumber as a function of $\beta=Q^2$. The asymptotic behavior of γ_{0C} for $Q\to\infty$ is $\gamma_{0C}\sim\sqrt{2}/Q$.

Let us return now to the driven pendulum at low driving frequencies $\omega \ll Q^{-1}$. In this limit the pendulum responds adiabatically and experiences the motions described above. Thus, for $\gamma_1 \geq 1$ the pendulum successively rotates and oscillates as shown in Fig. 10(a) or 10(b) (evidently with positive and negative rotations). Since the driving period is much longer than the damping time of the oscillations, as the drive amplitude passes through zero the pendulum almost reaches its equilibrium position before the next rotation. Paradoxically, in this low-frequency region where the pendulum follows the excitation in a more or less adiabatical way, a chaotic state exists.

As already intimated above, the crucial point in

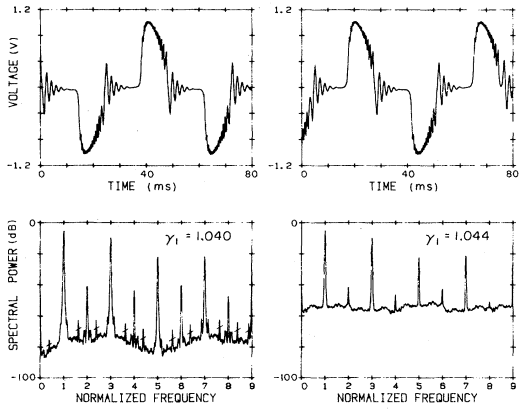

FIG. 10. Observed temporal voltage traces and associated spectral power of the chaotic and nonchaotic states observed at low driving frequencies. Note that in this figure the frequency is normalized to the driving frequency ($\omega=0.034$), not the natural frequency of the circuit and that the spectral lines with slash marks are due to 50-Hz pick-up.

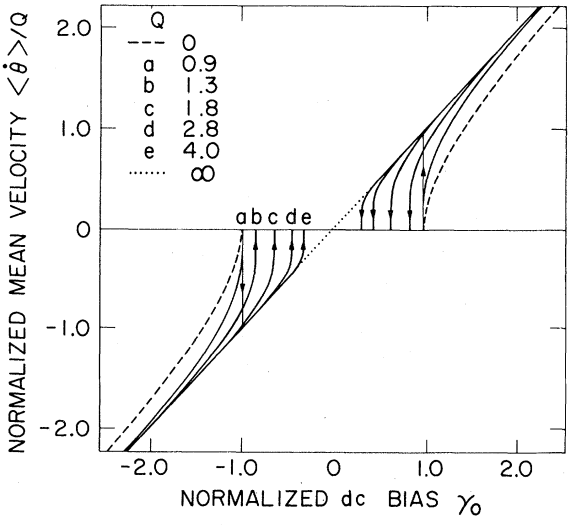

FIG. 11. Traces of the dc response of the simulator circuit as a function of finite dc bias γ_0 for various values of Q.

the dynamics of the pendulum associated with the observed chaos at these low frequencies is the transition from rotation to ringing down. More specifically, it is the occasional "extra" rotations [see transition on the far right of Fig. 10(b)] that lead to the observed noise. Apparently, for particular values of γ_1, the ringing-down portion of the cycle becomes very sensitive to the exact manner (i.e., the "initial conditions") in which the ringing down begins. Moreover, as for the period doubling seen on the phase-locked steps, the "dangerous" part of the orbit is when the pendulum approaches the unstable position with small angular velocity. Unfortunately, none of the general modes of chaos with which we are familiar seem able to describe this type of chaotic state.

B. Intermediate frequencies—intermittency between unstable phase-locked states

As shown in Fig. 3, in between the phase-locked states there are chaotic regions where, as seen in Fig. 1, the noise spectrum is finite even at dc. The chaotic stripes appear to be associated with intermittency between unstable phase-locked states. Similar intermittent behavior has been noted by Kautz[2] and by Ben-Jacob and co-workers[10,11] in the present of a dc bias.

A typical noise spectrum of one of these regions was shown in Fig. 6(c). The spectrum has two important characteristics. First of all, it extends down to dc, as already noted. Second, it has an amplitude which is much larger than the noise associated with the period-doubling cascade. [Compare Figs. 6(b) and 6(c).] Finally, it exhibits broad "resonances" centered around the unstable periodic phase-locked orbits, the width of which are presumably related to the lifetime of the periodic states.

In Fig. 12 we show the phase-space portrait of one of these chaotic states [Fig. 12(b)] compared with those of the phase-locked states between which it is observed [Figs. 12(a) and 12(c)]. It is clear from the figure that in this particular type of chaotic state, the motion involved can be viewed as an intermittency between two unstable phase-locked states as asserted above. Figure 13 shows another example of such a chaotic state [Fig. 13(a)], along with its associated Poincaré section [Fig. 13(b)] and those of the closest phase-locked states [Fig. 13(c)], with γ_1 adjusted so as to bias them in a chaotic condition. In our experiment, the Poincaré section of the intermittent states was always found to have the structure illustrated in this figure, namely, two

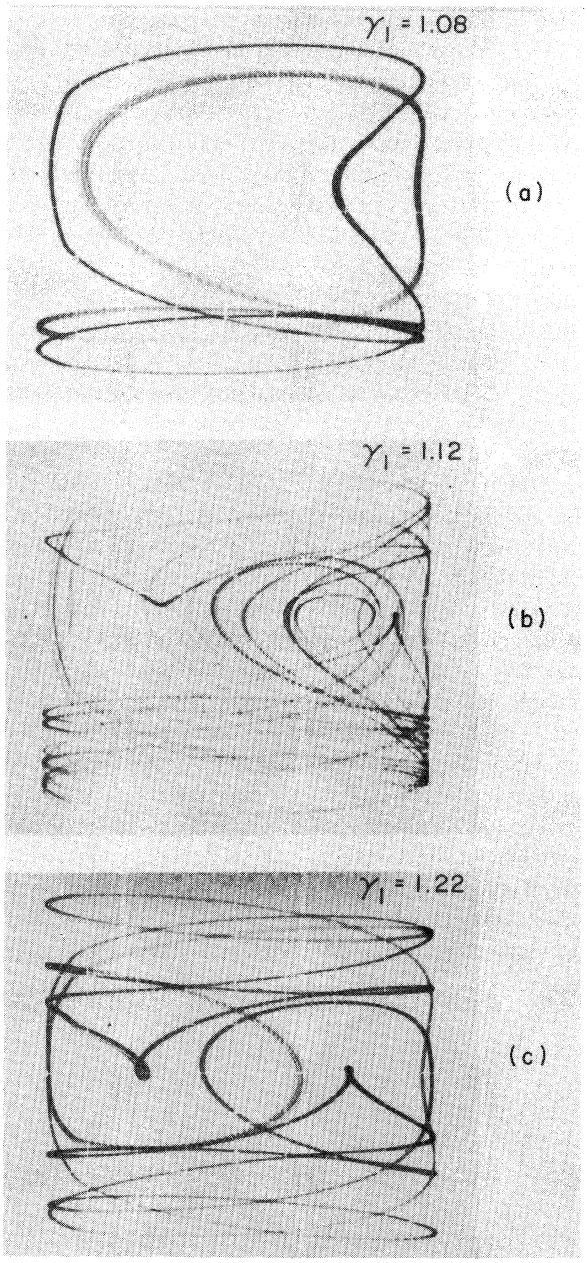

FIG. 12. Phase-space portraits of an intermittent state (b) along with the two nearby phase-locked states [(a) and (c)] to which it is related.

strange attractors connected by an important transient, even if the intermittent state was entered directly from a purely periodic state. Hence, Fig. 13 illustrates the important role phase noise plays in this intermittent state. Specifically, the presence of the strange attractors of phase-locked states could be the signature of an important phase randomization after each change of state. Note, however, that careful examination of Fig. 13(b) shows that the

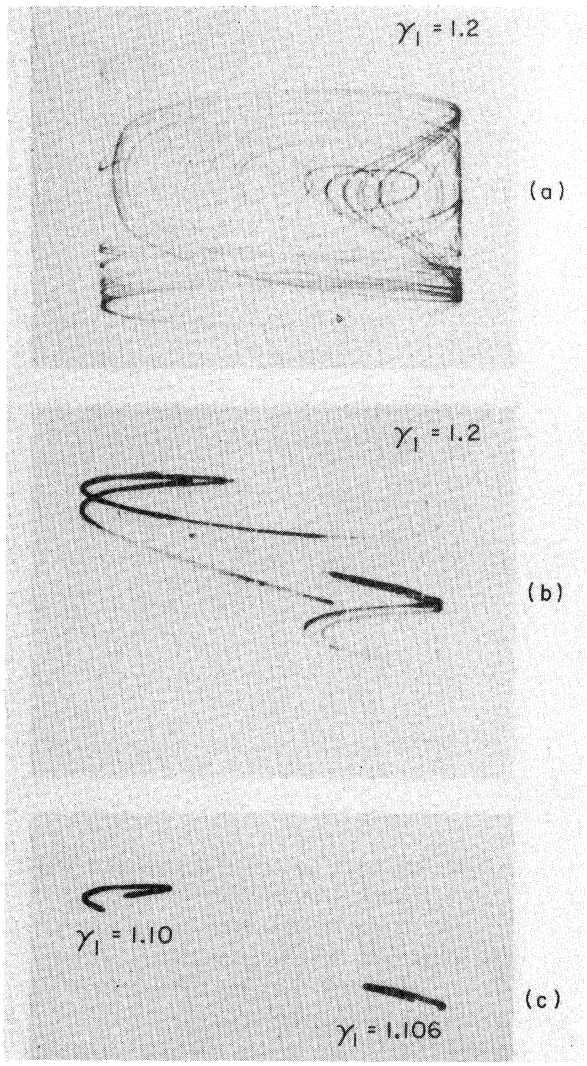

FIG. 13. Another example of the (a) phase-space portrait of an intermittent state, (b) along with its corresponding Poincaré section, (c) and the Poincaré sections of the two phase-locked states to which it is related. Note also the twofold structure in the Poincaré section of (b). These Poincaré sections were obtained directly from oscilloscope traces by means of a z-axis modulation synchronized to the drive signal.

Poincaré section of the full intermittent state has a double-line structure like that found in strange attractors derived from two-dimensional mappings of the Henon-type.[12] This double-line structure is not present in the related Poincaré sections of Fig. 13(c).

To date we have not found a model or mapping that properly describes this intermittent state. The model of Ben-Jacob, Goldhirsh, and Imry[11] has many of the features we observe but does not include the random-phase noise at the start of each laminarlike segment that is seen experimentally. We feel this phase noise is an essential feature of the observed behavior. This intermittency may be related to tangent bifurcations such as discussed by Yorke and Yorke[13] and Manneville and Pomeau[14] but it does not agree with the particular case analyzed in detail by Hirsh, Huberman, and Scalapino,[15] which deals with the familiar one-dimensional map with a quadratic maximum. In this latter case, as the control parameter is increased, the intermittency is followed by an odd period-doubling cascade—a behavior not seen in our experiments. The connection between the observed behavior and the sinusoidal map (which does exhibit periodic running solutions and multiwell diffusion) discussed recently by various authors,[16–18] is also not yet clear. Finally, in a somewhat unrelated vein, we note that nowhere in our experiment have we observed the quasiperiodic route to chaos proposed by Ruelle and Takens.[19]

VI. EFFECT OF dc BIAS

The presence of a dc bias γ_0 strongly influences the response of the pendulum to a periodic driving force, but to the extent that we have been able to establish, it does not introduce any fundamentally different states or new types of chaos. That is, there are both phase-locked and -unlocked states of the type found in zero-bias as shown in Fig. 3. The phase-locked states correspond to ac Josephson steps and the unlocked states can be intermittent. Smooth transitions between phase-locked states are also observed under some conditions as the dc bias is increased, but they correspond to the uninteresting situation where there is no interaction (i.e., locking or tendency to lock) between the drive frequency and the average rotation frequency of the pendulum. The power spectrum under these conditions consists of lines at the drive frequency, the rotation frequency, their harmonics and mixing products, with no subharmonics or broadband noise.

The effect of a small dc bias (i.e., biasing within a given potential well) is simple and easy to understand. It has four principal effects. External symmetry breaking is introduced, the resonant frequency is lowered, the quality factor is decreased, and the critical ac torque required to produce rotation is reduced. This behavior can be understood trivially in terms of the linear ac response expected for a biased pendulum. The equilibrium position is given by $\theta_0 = \sin^{-1}\gamma_0$, from which it follows that $\omega_0 \to (1-\gamma_0^2)^{1/4}$ and $Q \to Q(1-\gamma_0^2)^{1/4}$. The net ef-

fect of all this is, roughly speaking, simply to scale the state diagram of Fig. 3 along the γ_1 and ω axes. Note, however, that as $\gamma_0 \to 1$, $Q \to 0$ and one expects the structure in the state diagram to be strongly modified and eventually all chaotic behavior to cease. This limit was not carefully explored in our study.

ACKNOWLEDGMENTS

Two of us (M.R.B. and B.A.H.) would like to thank all of the members of the Groupe de Physique des Solides de l'Ecole Normale Superieure for having provided both the facilities and the warm hospitality that made this collaboration possible. All of us would like to express our thanks to A. Launay for his invaluable technical help with the development of the circuits used in these experiments. Finally, one of us (M.R.B.) would like to acknowledge the support of the U. S. National Science Foundation during the final stages of the completion of this work.

APPENDIX A: SIMULATOR CIRCUIT

To simulate a driven pendulum we have used an analog circuit of the phase-locked-loop variety described by Bak[20] in the context of a simulator for the resistively shunted junction model of a Josephson junction. The basic functional diagram of the circuit is shown in Fig. 14 and the detailed circuit diagram in Fig. 15. In the circuit the output of a voltage-controlled oscillator (VCO) is mixed with a reference oscillator, passed through a low-pass filter, and then fed back to the input of the VCO through an operational amplifier. The ac and dc bias inputs are applied at the summing point of the operational amplifier. The resistor and capacitor in the feedback circuit of the operational amplifier provide the inertia and damping of the loop.

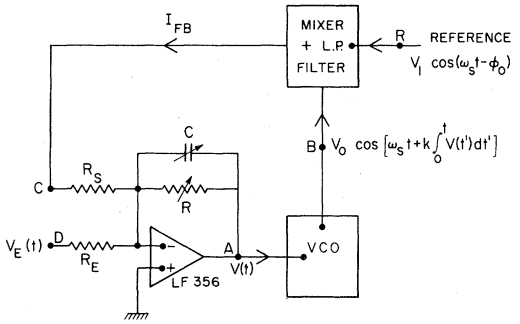

FIG. 14. Schematic diagram of the phase-locked loop used in our simulations. Typical circuit values are $R=11$ kΩ, $C=100$ nF, $k=4\pi\times10^3$ s^{-1}/V which lead to a natural frequency $\Omega_0/2\pi=600$ Hz and a $Q=4$. We also used $R_E=R_S=10$ kΩ and a reference frequency $\omega_s/2\pi=100$ kHz.

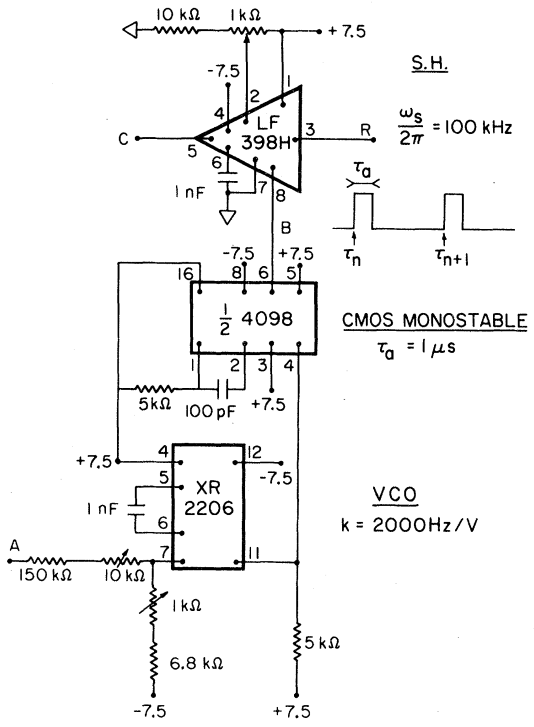

FIG. 15. Detailed circuit diagram for phase-locked loop.

In practice, the actual circuit we used was patterned after that developed by Henry and Prober,[21] in which the mixing and low-pass filtering functions are accomplished using a sample-and-hold (SH) circuit. The merits and demerits of this approach have been discussed by those authors.

If the reference signal is $V_1\sin(\omega_s t+\phi_0)$, the output of the sample-and-hold circuit sampled at the time τ_n is $V_1\sin(\omega_s\tau_n+\phi_0)$. During the hold time between τ_n and the next sampling time τ_{n+1}, the input $V(t)$ of the VCO is given by

$$\frac{1}{C}\frac{dV}{dt}+\frac{1}{R}V+\frac{V_1}{R_S}\sin(\omega_s\tau_n+\phi_0)=-\frac{V_E(t)}{R_E}\ . \tag{A1}$$

The sampling time τ_{n+1} is related to τ_n and to the input of the VCO by

$$\omega_s(\tau_{n+1}-\tau_n)+k\int_{\tau_n}^{\tau_{n+1}}V(t)dt=2\pi\ . \tag{A2}$$

Writing

$$\theta_n=(2n+1)\pi-\omega_s\tau_n-\phi_0 \tag{A3}$$

one gets

$$\theta_{n+1}=\theta_n+2\pi-\omega_s(\tau_{n+1}-\tau_n)$$
$$=\theta_n+k\int_{\tau_n}^{\tau_{n+1}}V(t)dt\ . \tag{A4}$$

If ω_s is larger than the highest frequency of $V(t)$ during the time between τ_n and τ_{n+1}, $V(t)$ can be considered as constant and written

$$V(t)=\lim_{\omega_s\to\infty}\left[\frac{1}{k}\left[\frac{\theta_{n+1}-\theta_n}{\tau_{n+1}-\tau_n}\right]\right]=\frac{\dot\theta}{k}\ . \tag{A5}$$

So, if one could neglect the time between sampling, one gets

$$\dot\theta=kV(t)\ , \tag{A6}$$

$$C\frac{dV}{dt}+\frac{1}{R}V+\frac{V_1}{R_S}\sin\theta=-\frac{V_E(t)}{R_E}\ , \tag{A7}$$

or

$$\frac{C}{k}\ddot\theta+\frac{1}{kR}\dot\theta+\frac{V_1}{R_S}\sin\theta=-\frac{V_E(t)}{R_E}\ , \tag{A8}$$

where V_1 is the peak amplitude of the reference. With the notations of Sec. II one gets

$$a=C/k,\quad b=1/kR,\quad c=V_1/R_S\ ,$$
$$\Gamma(t)=-V_E(t)/R_E\ .$$

It is also interesting to note, referring back to Eq. (A4), that for a periodic $V(t)$ the integral of $V(t)$ can be calculated explicitly and then Eq. (A4) becomes a discrete mapping reflecting the actual behavior of an ideal VCO fed back through an ideal sample-and-hold circuit.

From the simulation point of view, this circuit has two drawbacks associated with the detailed operation of the sample-and-hold circuit. Specifically, because of the finite aperture time and an overshoot in the response of the SH, the sampling transient leads to an error in $I_{\rm FB}$ that depends on the phase between the VCO and the reference signal. An important consequence of this problem is the introduction of two discontinuities in the slope of $I_{\rm FB}$ near its extrema and of an asymmetry in the amplitude of $I_{\rm FB}$ between its positive and negative half-cycles. Note, however, that while such asymmetries may dictate which way the symmetry breaking of the simulated pendulum goes, by carefully studying the effects of an applied dc bias, we conclude that the observed symmetry breaking is intrinsic to the forced pendulum and not an idiosyncrasy of our simulator circuit.

APPENDIX B: STABILITY OF PHASE-LOCKED STEPS

In Sec. IV we have investigated solutions of Eq. (3) of the form

$$\theta^*=\theta_n+n(\omega\tau-\phi)-\alpha\sin(\omega\tau-\phi) \tag{B1}$$

with θ_n, α, and ϕ related to γ_0, γ_1, and n by Eqs. (13)–(15). Such solutions will be observed only if they are stable, i.e., only if any small perturbation $\delta\theta$ of θ^* is damped. Writing $\theta=\theta^*+\delta\theta$, for $\delta\theta\ll1$ one gets

$$\delta\ddot\theta+\frac{1}{Q}\delta\dot\theta+\cos\theta^*\delta\theta=0\ . \tag{B2}$$

Limiting the $\cos\theta^*$ expansion to the first two terms, one obtains the following Mathieu equation:

$$\frac{d^2y}{dz^2}+(a-2q\cos2z)y=0\ , \tag{B3}$$

where

$$a=\frac{4}{\omega^2}\left[J_n(\alpha)\cos\theta_n-\left[\frac{1}{2Q}\right]^2\right]\ , \tag{B4}$$

$$q=\frac{4}{\omega^2}\left[\left[\frac{n}{\alpha}-J_n(\alpha)\cos\theta_n\right]^2+[J_n'(\alpha)\sin\theta_n]^2\right]^{1/2}\ , \tag{B5}$$

$$z=\tfrac{1}{2}(\omega\tau-\phi+\nu_n)\ , \tag{B6}$$

$$y=\delta\theta\,e^{-\tau/2Q}\ , \tag{B7}$$

$$\tan\nu_n=\alpha J_n'(\alpha)\tan\theta_n/nJ_n(\alpha)\ . \tag{B8}$$

However, if $n=0$ and $\gamma_0=0$, then $\theta_n=0$, Eq. (B5) leads to $q=0$, and the expansion of $\cos\theta^*$ must be taken one order higher in which case (B4)–(B6) are replaced by

$$a=\frac{1}{\omega^2}\left[J_0(\alpha)-\frac{1}{(2Q)^2}\right]\ , \tag{B9}$$

$$q=\frac{1}{\omega^2}J_2(\alpha)\ , \tag{B10}$$

$$z=\omega\tau-\phi\ . \tag{B11}$$

Hence, we find that the stability of θ^* will have the same kind of behavior[22] as the solutions of the cor-

responding Mathieu equation. If a and q belong in the stability domain of the Mathieu equation,[23] θ^* is stable. If, on the other hand, the solutions of Eq. (B3) are unstable, only two kinds of bifurcations can occur, either with period π or 2π for z. Now the interpretation of these bifurcations depends on the symmetry of θ^*. If $n=0$ and $\gamma_0=0$, z and $\omega\tau$ are related by Eq. (B11) and the bifurcations occurs with periods ω or 2ω. The first case corresponds to a jump toward another stable state still given by Eq. (B1) (if one exists). A vivid illustration of this bifurcation is given in Figs. 4 and 7, where the negative slope part of the S-shaped resonance is unstable, leading to the hysteretic behavior in Fig. 4. When the other bifurcation occurs, the solution of (B2), which grows, has a frequency twice the drive frequency and, as a consequence, a dc component.[23] Hence, in this case, the system goes to a state where $\langle\theta\rangle$ is nonzero and this bifurcation corresponds to a symmetry breaking of the pendulum motion for $\gamma_0=0$. If $n\neq 0$ or $\gamma_0\neq 0$, then the motion of the pendulum is already asymmetric, z and $\omega\tau$ are related by Eq. (B6), and the bifurcations occur with periods ω or $\omega/2$. The first one was described above. The second corresponds to a growth of solution with frequency half the drive frequency, i.e., to period doubling.

From this analysis we conclude that, for the forced pendulum, before any period-doubling bifurcation the symmetry of the motion must be broken either with an external torque γ_0 or by a previous bifurcation.

---

*Permanent address: Department of Applied Physics, Stanford University, Stanford, California 94305.

†Permanent address: Xerox Palo Alto Research Center, Palo Alto, California 94304.

[1]B. A. Huberman, J. P. Crutchfield, and N. Packard, Appl. Phys. Lett. 37, 750 (1980).

[2]R. C. Kautz, J. Appl. Phys. 52, 624 (1981).

[3]N. F. Pedersen and A. Davidson, Appl. Phys. Lett. 39, 830 (1981).

[4]B. A. Huberman and J. P. Crutchfield, Phys. Rev. Lett. 43, 1743 (1979).

[5]A. Libchaber and J. Maurer, J. Phys. Coll. 41, 51 (1980).

[6]A. Arneodo, P. Coullet, C. Tresser, A. Libchaber, J. Maurer, and D. d'Humieres (unpublished).

[7]M. J. Feigenbaum, Phys. Lett. 74A, 375 (1979).

[8]N. F. Pedersen, O. H. Soerensen, B. Dueholm, and J. Mygend, J. Low. Temp. Phys. 38, 1 (1980).

[9]D. E. McCumber, J. Appl. Phys. 39, 3113 (1968).

[10]E. Ben Jacob, Y. Braiman, and R. Shainsky, Appl. Phys. Lett. 38, 822 (1981).

[11]E. Ben Jacob, I. Goldhirsh, and Y. Imry (unpublished).

[12]E. Henon, Commun. Math. Phys. 50, 69 (1976).

[13]J. A. Yorke and E. D. Yorke, J. Stat. Phys. 21, 263 (1979).

[14]P. Manneville and Y. Pomeau, Phys. Lett. 75A, 1 (1979).

[15]J. E. Hirsh, B. A. Huberman, and D. J. Scalapino, Phys. Rev. A 25, 519 (1982).

[16]T. Geisel and J. Nierwetberg, Phys. Rev. Lett. 48, 7 (1982).

[17]S. Grossman (unpublished).

[18]M. Schell, S. Fraser, and R. Kapral (unpublished).

[19]D. Ruelle and F. Takens, Commun. Math. Phys. 20, 167 (1970).

[20]C. K. Bak and N. F. Pedersen, Appl. Phys. Lett. 22, 149 (1973).

[21]R. W. Henry and D. E. Prober, Rev. Sci. Instrum. 52, 912 (1981).

[22]We must point out that Eq. (B3) is only an approximation of Eq. (B2). As a consequence, the choice between sets of Eqs. (B4)–(B8) or Eqs. (B9)–(B11) is not exactly given by conditions $n=0$, $\gamma_0=0$ but by comparison between the value of q given by Eqs. (B5) and (B10) with a domain where the two values are close and in which Eq. (B3) cannot describe the stability of θ^*.

[23]*Handbook of Mathematical Functions*, 7th ed., edited by M. Abromowitz and I. Stegun (Dover, New York, 1970), p. 721.

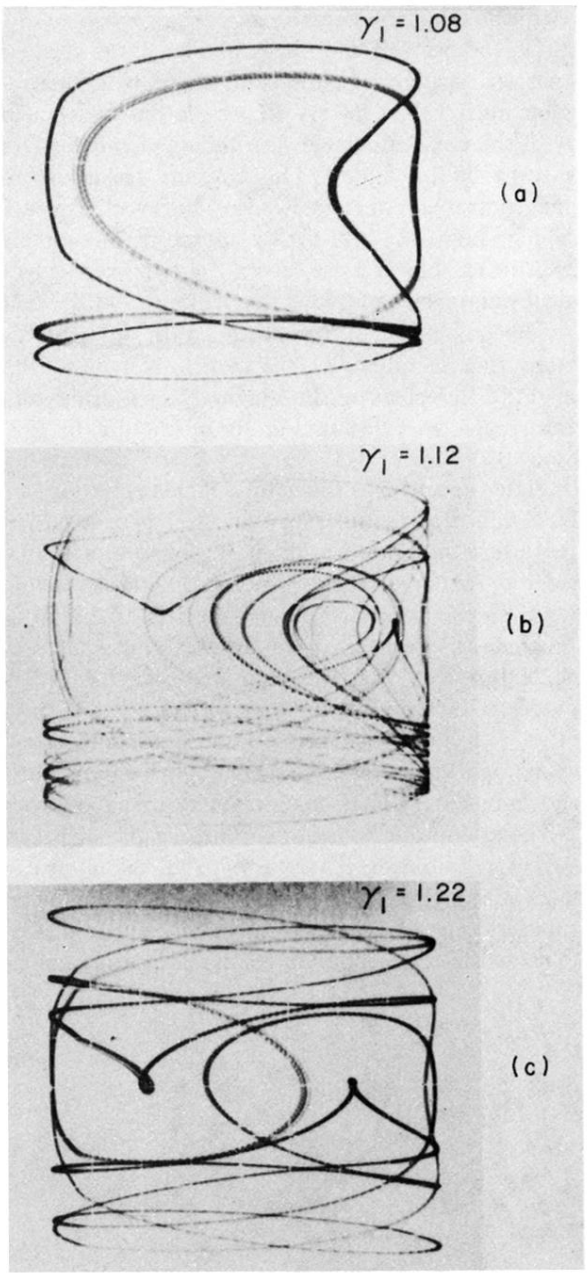

FIG. 12. Phase-space portraits of an intermittent state (b) along with the two nearby phase-locked states [(a) and (c)] to which it is related.

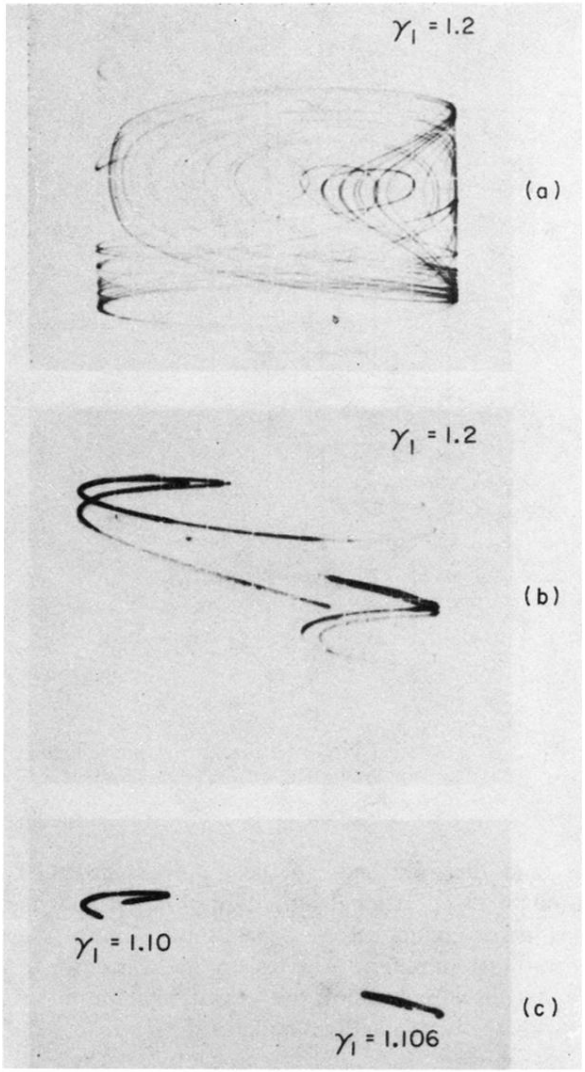

FIG. 13. Another example of the (a) phase-space portrait of an intermittent state, (b) along with its corresponding Poincaré section, (c) and the Poincaré sections of the two phase-locked states to which it is related. Note also the twofold structure in the Poincaré section of (b). These Poincaré sections were obtained directly from oscilloscope traces by means of a z-axis modulation synchronized to the drive signal.

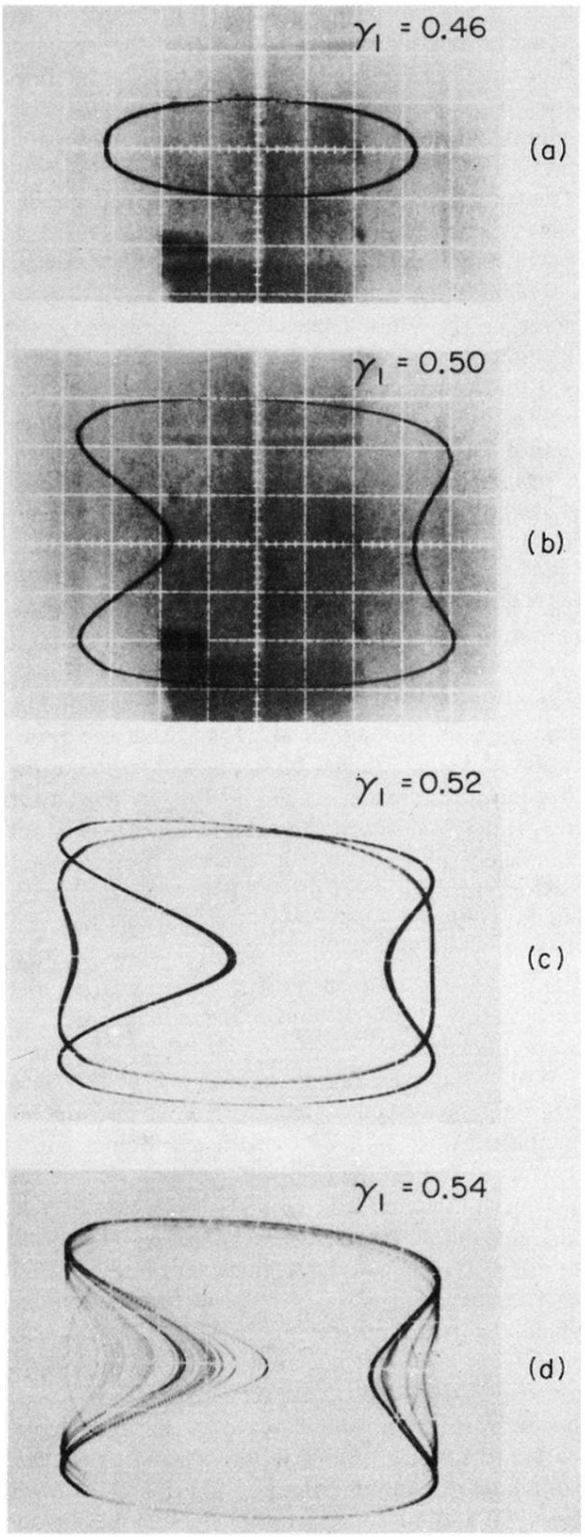

FIG. 5. (a) Evolution of the phase-space portraits ($\dot{\theta}$ vs $\sin\theta$) for increasing driving amplitude γ_1 at fixed frequency $\omega=0.67$. (b) Note the symmetry breaking, (c) followed by period doubling, (d) followed by chaos.

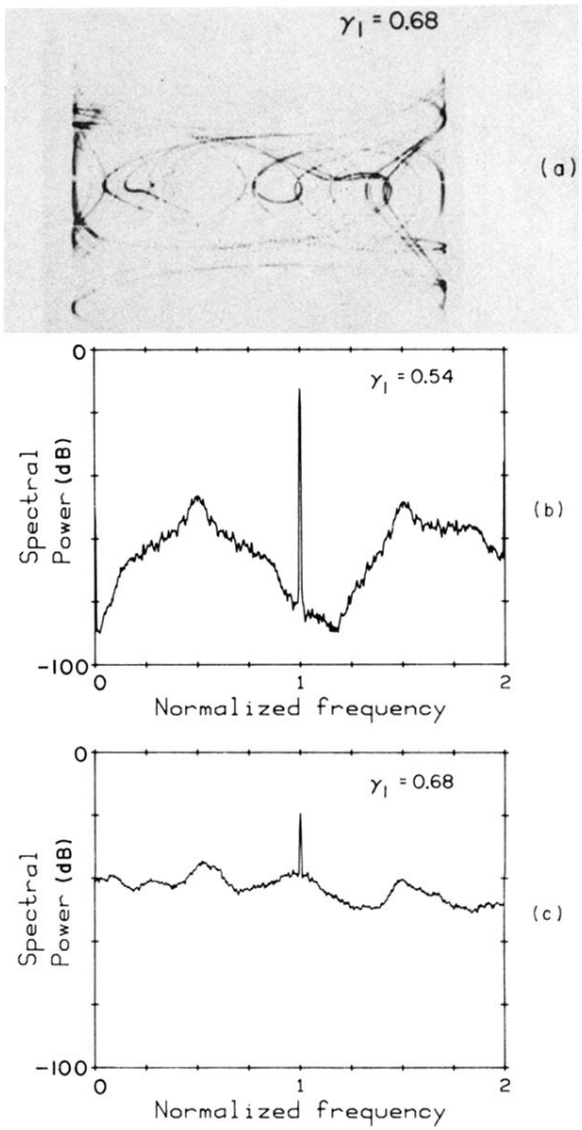

FIG. 6. (a) Phase-space portrait corresponding to the intermittent domain of Fig. 3 at $\omega=0.67$. (b) and (c) show the spectral power density corresponding to Figs. 4(d) and 5(a). Note different behavior as $\omega \rightarrow 0$. Note also that in this figure and all other power spectra the frequency axis is normalized to the drive frequency.

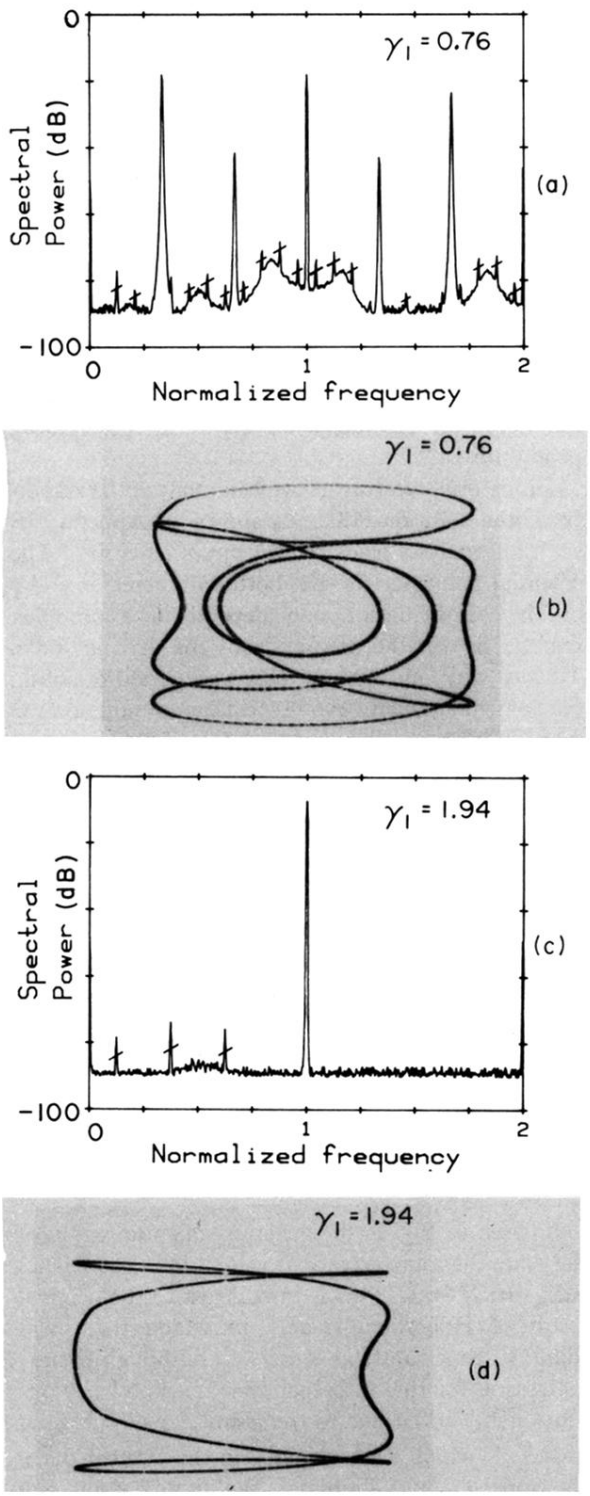

FIG. 8. Phase-space portraits and associated spectral power for two symmetric ($n=0$) large-amplitude rotating states. (a) and (b) correspond to a period-tripled state. (c) and (d) correspond to a simple period-one state. Note that the spectral lines with slash marks are due to 50-Hz pick-up.

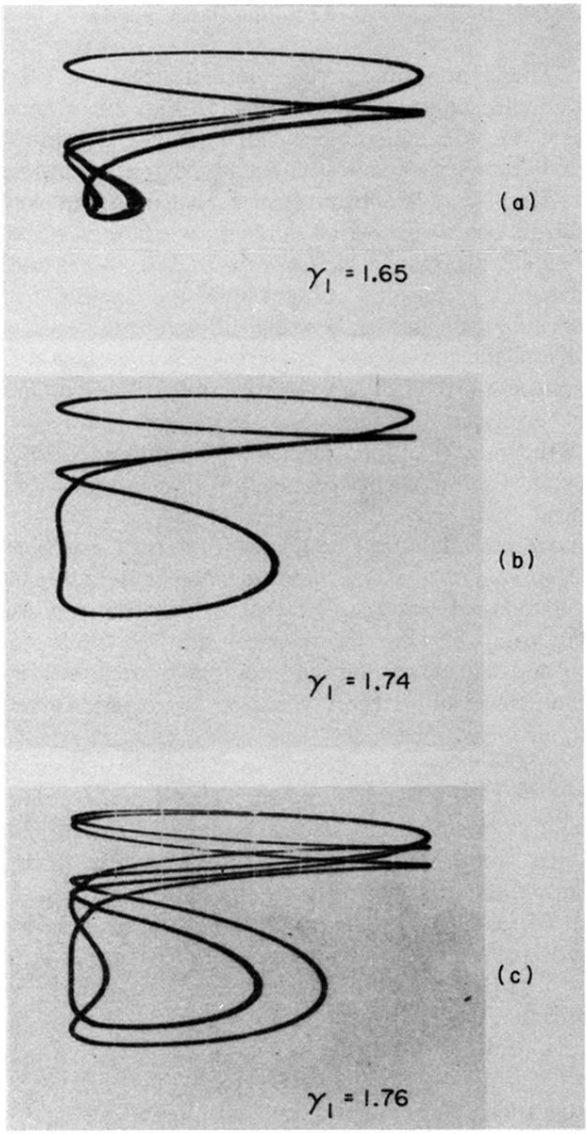

FIG. 9. Phase-space portraits of phase-locked periodic running states ($n \geq 1$) illustrating nonmonotonic period-doubling pitch fork bifurcations.